Available online at www.sciencedirect.com
ScienceDirect
Ceramics International 35 (2009) 2619–2623
CERAMICS INTERNATIONAL
www.elsevier.com/locate/ceramint

Energy transfer and up-conversion luminescence in Er^{3+}/Yb^{3+} co-doped transparent glass ceramic containing YF_3 nano-crystals

Fangyi Weng, Daqin Chen, Yuansheng Wang *, Yulong Yu, Ping Huang, Hang Lin

State Key Laboratory of Structural Chemistry, Fujian Institute of Research on the Structure of Matter, Chinese Academy of Sciences, Graduate School of Chinese Academy of Sciences, Fuzhou, Fujian 350002, China

Received 3 December 2008; received in revised form 5 February 2009; accepted 27 February 2009
Available online 27 March 2009

Abstract

Transparent glass ceramics containing YF_3 nano-crystals were fabricated by heat treatment of the SiO_2–Al_2O_3–NaF–YF_3–LnF_3 (Ln = Er, Yb) glasses. X-ray diffraction and transmission electron microscopy analyses evidenced the homogeneous distribution of spherical YF_3 nano-crystals sized 25–30 nm among the glassy matrix. Energy dispersive X-ray spectroscopy measurement, combined with the Stark splitting of the absorption and emission bands, verified the incorporation of Er^{3+} and Yb^{3+} ions into YF_3 nano-crystals. The infrared to visible up-conversion emission of Er^{3+} intensified with the increasing of Yb^{3+} concentration, ascribing to the increase of the efficiency of non-radiative energy transfer from Yb^{3+} to Er^{3+} which exceeded 45% for the $0.5Er^{3+}/1.0Yb^{3+}$ co-doped sample. The up-conversion luminescence at 545 and 660 nm were affirmed coming from two-photon excitation process.

Keywords: B. Nanocomposites; B. Spectroscopy; C. Optical properties; D. Glass ceramic

1. Introduction

In recent years, the rare earth (RE) doped optical materials have been extensively investigated due to their potential applications in many fields, such as color display, optical data storage, sensor, laser and optical amplifier for communication [1–5]. Among the trivalent RE ions, Er^{3+} attracted much attention for its useful up-conversion characteristic [6,7]. However, the low absorption cross-section of Er^{3+} around 980 nm limits its further commercial applications. Yb^{3+}, having a high and broad absorption band matching well with the emission wavelength of the InGaAs laser diode, was reported as an excellent sensitizer for the Er^{3+}-activated optical materials [5,8].

It is well known that, as the host for the luminescent RE, fluoride is preferable over oxide mainly for the lower phonon energy to avoid non-radiative transition of RE ions [9]. However, the synthesis of fluoride crystals is complicated, and the stability and fiberizability as practical materials still remain problematic. A good solution would be the oxyfluoride glass ceramic with fluoride nano-crystallites embedding among an oxide glassy matrix of high chemical and mechanical stabilities [10–13]. The advantages of this material are that the RE ions would be incorporated selectively into the fluoride crystalline phase during the course of controlled crystallization, and good transparency is maintained due to much smaller of the crystal size than the wavelength of the visible light [14]. In this work, the Er^{3+}/Yb^{3+} co-doped glass ceramics containing YF_3 nano-crystals were fabricated, and the partition, the infrared and up-conversion fluorescence, as well as the energy transfer processes, of the RE ions were studied.

2. Experimental

The Er^{3+}/Yb^{3+} co-doped precursor glasses were prepared with the following composition (in mol%): $44SiO_2$–$28Al_2O_3$–$17NaF$–$11YF_3$–$xErF_3$–$yYbF_3$ ($x = 0$, 0.1, 0.5; $y = 0$, 0.1, 0.2, 0.4, 0.8, 1.0, respectively). All the raw materials are of analytical reagent grade. For each batch, about 15 g of starting materials were fully mixed, and melted in a covered corundum crucible in air atmosphere at 1450 for 1 h, and then cast into a brass mold, followed by annealing to relinquish the inner stress.

* Corresponding author. Tel.: +86 591 8370 5402; fax: +86 591 8370 5402.
E-mail address: yswang@fjirsm.ac.cn (Y. Wang).

0272-8842/$36.00
doi:10.1016/j.ceramint.2009.02.026

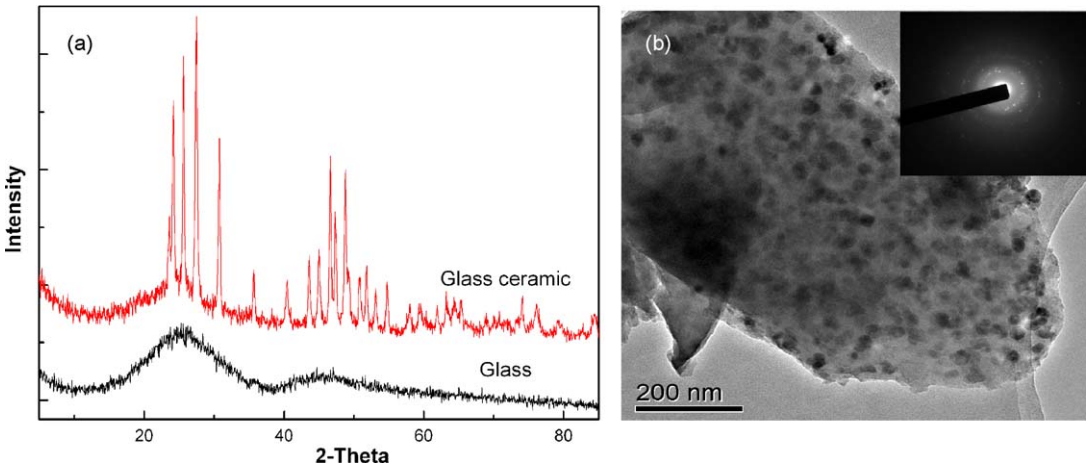

Fig. 1. XRD patterns of the precursor glass and glass ceramic (a), and TEM micrograph of the glass ceramic (b).

The precursor glasses thus obtained were cut into squared samples with thickness of 3 mm, which were heat-treated subsequently at 670 for 2 h to induce crystallization.

To characterize the crystallization phase, X-ray diffraction (XRD, DMAX2500 RIGAKU with Cu Kα radiation, the resolution is 0.01°) and transmission electron microscopy (TEM, JEM-2010 equipped with an energy dispersive X-ray spectroscopy system) observation were carried out. The absorption spectra were recorded on a spectrophotometer (Lambda900, PerkinElmer) with a spectral range from 200 to 2000 nm and a resolution of 1.0 nm. By using an InP/InGaAs photomultiplier tubes (PMT) detector (R5509), the infrared luminescence signals through the emission monochromator (M300) were measured. The fluorescence decay curves were recorded with a NIR PMT (R5509) excited by a microsecond flash lamp (μF900). The visible up-conversion luminescence excited with a 30 mW diode laser at 980 nm was measured with a PMT detector (R928). All the measurements were carried out at room temperature.

3. Results and discussion

3.1. Microstructure

XRD pattern shown in Fig. 1(a) evidences the amorphous structure of the precursor glass. For the pattern taken from the heat-treated sample, there are several sharp diffraction peaks which can be readily indexed by the orthorhombic YF_3 (PDF 32-1431), indicating the precipitation of YF_3 in the sample. The mean size of YF_3 crystallites was estimated to be about 28 nm by Scherrer's equation. The TEM micrograph of the glass ceramic demonstrates that YF_3 nano-crystals sized about 30 nm are distributed homogeneously among the glassy matrix, as shown in Fig. 1(b), in consistent with the XRD results.

The absorption spectra of the $0.1Er^{3+}/1.0Yb^{3+}$ co-doped glass and glass ceramic in the 350–1650 nm region are shown in Fig. 2. Due to the strong absorption of the host matrix in the ultraviolet range, the absorption band at wavelength shorter than 350 nm could not be distinguished. The absorption bands are assigned to the transitions from Er^{3+} $^4I_{15/2}$ ground state to the excited states. The broad absorption band in the range of 870–1100 nm corresponds to the superposition of Er^{3+}: $^4I_{15/2} \rightarrow {}^4I_{11/2}$ and Yb^{3+}: $^2F_{7/2} \rightarrow {}^2F_{5/2}$ transitions. Compared with those of the precursor glass, the absorption coefficients for the transitions of Er^{3+} and Yb^{3+} from the ground states to the excitation states (e.g., Er^{3+}: $^4I_{15/2} \rightarrow {}^4I_{11/2}$ and Yb^{3+}: $^2F_{7/2} \rightarrow {}^2F_{5/2}$) of the glass ceramic decrease remarkably, and the absorption bands around 980 and 1520 nm become structured, suggesting the incorporation of Er^{3+} and Yb^{3+} ions into YF_3 nano-crystals after crystallization.

In order to detect directly the distribution of RE ions in the glass ceramic, energy dispersive X-ray spectroscopy (EDS) analyses with nano-sized probe on the glassy matrix and an individual nano-crystal in the $0.1Er^{3+}/1.0Yb^{3+}$ co-doped glass ceramic were conducted (the diameter of the electron probe was adjusted to 5–10 nm. Considering the possible expansion of the electron beam when it penetrated through the detecting area, the special resolution of the EDS analysis is deemed to be in the range of 10–20 nm). The spectrum from the glassy matrix,

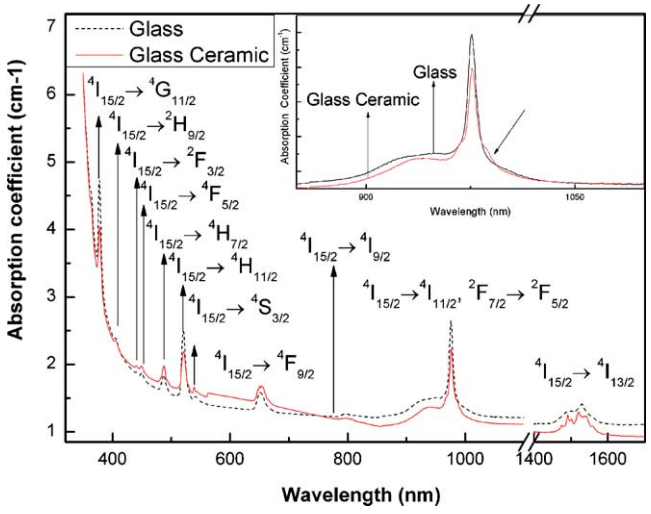

Fig. 2. Absorption spectra from the $0.1Er^{3+}/1.0Yb^{3+}$ co-doped glass and glass ceramic; the inset shows the absorption band in the range of 870–1100 nm corresponding to the superposition of Er^{3+}: $^4I_{15/2} \rightarrow {}^4I_{11/2}$ and Yb^{3+}: $^2F_{7/2} \rightarrow {}^2F_{5/2}$ transitions.

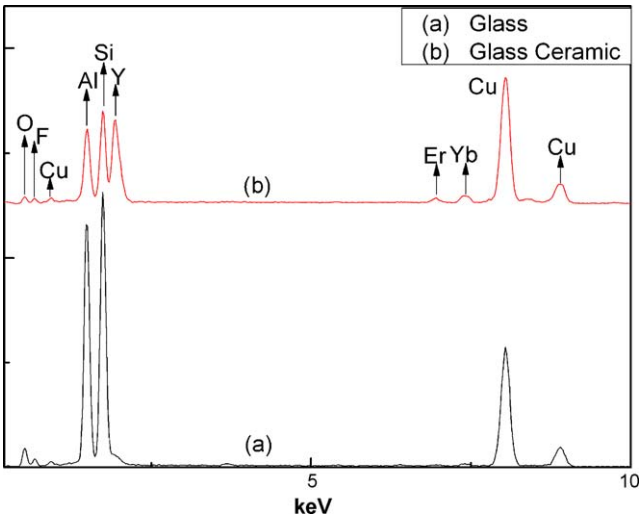

Fig. 3. EDS spectra from the glassy matrix (a), and an individual YF_3 nano-crystal (b), in the $0.1Er^{3+}/1.0Yb^{3+}$ co-doped glass ceramic; the presence of Cu peaks is due to the copper grid used to support TEM specimen.

presented in Fig. 3(a), shows high content of Si, O, Al, and small amount of residual Y, F and Yb, while Er content is under the detecting limit. As a comparison, the spectrum from an individual nano-crystal, shown in Fig. 3(b), exhibits strong signals of Y, F, Er, and Yb (the Al, Si and O peaks are attributed to the matrix surrounding the nano-crystal). These results further confirm that Er^{3+} and Yb^{3+} ions are mainly concentrated in YF_3 nano-crystals.

3.2. Fluorescence properties

For the Er^{3+} single-doped or Er^{3+}/Yb^{3+} co-doped precursor glasses, no any up-conversion signals were detected. The up-conversion emission spectra of the Er^{3+}/Yb^{3+} co-doped glass ceramics with various Yb^{3+} concentrations under 980 nm excitation, detected with the same instrumental condition, are presented in Fig. 4. There are two up-conversion emission bands centered at 545 and 660 nm, corresponding to the $^2H_{11/2}$, $^4S_{3/2} \rightarrow {}^4I_{15/2}$ and $^4F_{9/2} \rightarrow {}^4I_{15/2}$ transitions of Er^{3+}, respectively, attributing to the energy transfer from Yb^{3+} to Er^{3+}. The green emission is dominant in all the co-doped glass ceramics. Significantly, with increasing of Yb^{3+} concentration, both green and red emissions intensify monotonously, indicating the enhanced probability of energy transfer from Yb^{3+} to Er^{3+}.

To investigate the excitation mechanism for the population of Er^{3+}: $^2H_{11/2}$, $^4S_{3/2}$ and $^4F_{9/2}$ levels after infrared excitation, we measured the power dependence of the up-conversion luminescence intensity. For an unsaturated up-conversion, the emission intensity is proportional to the nth power of the excitation intensity, and the integer n is the number of photons absorbed per up-converted photon emitted [15]. A plot of logarithm of the up-conversion intensity versus logarithm of the infrared excitation intensity should yield a straight line with slope n. Fig. 5 shows such a plot for the $0.1Er^{3+}/1.0Yb^{3+}$ co-doped glass ceramic with $n = 1.74$, 1.87 and 1.86 for Er^{3+}: $^2H_{11/2} \rightarrow {}^4I_{15/2}$, $^4S_{3/2} \rightarrow {}^4I_{15/2}$ and $^4F_{9/2} \rightarrow {}^4I_{15/2}$ transitions, respectively, of $0.1Er^{3+}/1.0Yb^{3+}$ co-doped glass ceramic. The values of n for all the transitions approach 2, indicating the two-photon mechanism for the up-conversion processes to populate Er^{3+}: $^2H_{11/2}$, $^4S_{3/2}$ and $^4F_{9/2}$ levels. The proposed mechanism for the infrared excitation and up-conversion emission are demonstrated in the schematic energy level diagram of Er^{3+} and Yb^{3+} ions, as shown in Fig. 6. In the first non-radiative energy transfer step, an Yb^{3+} ion in the $^2F_{7/2}$ ground state absorbs a 980 nm photon and to excite an electron to the $^2F_{5/2}$ state. When it drops back to the ground state, energy is transferred to an adjacent Er^{3+}: $^4I_{11/2}$ state. The second near infrared photon absorbed by the Yb^{3+} ion then pumps the Er^{3+} ion to a higher energy state of $^4F_{7/2}$, also through energy transfer from Yb^{3+} to Er^{3+}. Subsequently, a fast non-radiative relaxation from $^4F_{7/2}$ to $^2H_{11/2}$ and $^4S_{3/2}$ occurs and Er^{3+} ions then relax to the ground state by emitting the green luminescence. The red emission centered at 660 nm, shown in Fig. 4, ascribing to Er^{3+}: $^4F_{9/2} \rightarrow {}^4I_{15/2}$ radiative transition is very weak. The Er^{3+}: $^4F_{9/2}$ level is populated by the non-radiative decay from the $^2H_{11/2}$ and $^4S_{3/2}$ levels.

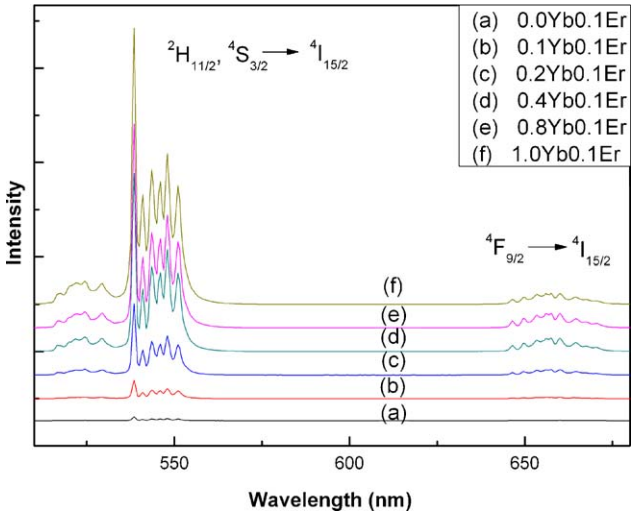

Fig. 4. Up-conversion emission spectra of the Er^{3+}/Yb^{3+} co-doped glass ceramics.

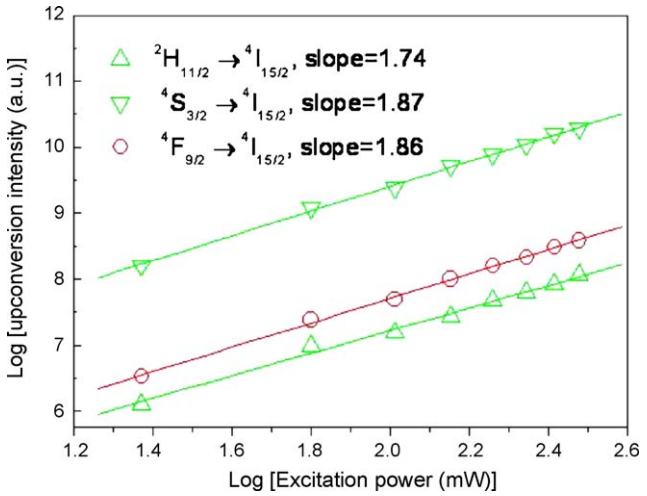

Fig. 5. Log–log plots of the up-conversion emission intensity vs. the excitation power for the $0.1Er^{3+}/1.0Yb^{3+}$ co-doped glass ceramic.

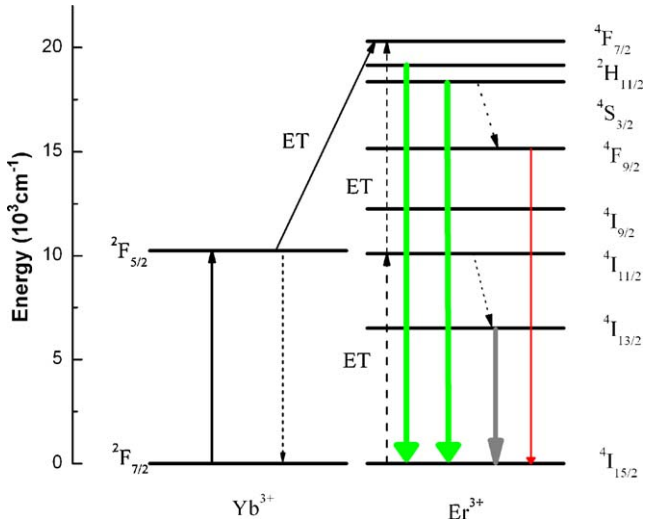

Fig. 6. Schematic energy level diagram of Yb^{3+} and Er^{3+}, showing the possible mechanism for the up-conversion emission of Er^{3+}.

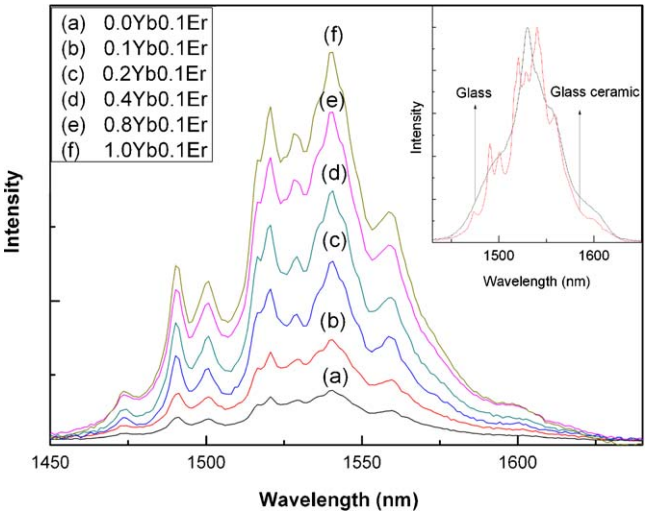

Fig. 7. Near-infrared fluorescence spectra of the Er^{3+}/Yb^{3+} co-doped glass ceramics with various Yb^{3+} concentration under 980 nm excitation; the inset shows line-shapes of 1.53 μm emission spectra of the precursor glass and Er^{3+}/Yb^{3+} co-doped glass ceramic.

Fig. 7 shows the near-infrared emission spectra around 1.53 μm for Er^{3+}: $^4I_{13/2} \rightarrow {}^4I_{15/2}$ transition under 980 nm excitation in the Er^{3+}/Yb^{3+} co-doped glass ceramics with various Yb^{3+} concentration. Compared with that of the precursor glass, remarkable Stark splits in the emission band of the glass ceramic, as shown in the inset of Fig. 7. Significantly, the 1.53 μm emission intensity enhances with increasing of the Yb^{3+} concentration, implying that the electron population in Er^{3+}: $^4I_{13/2}$ level, which is achieved by the non-radiative relaxation from $^4I_{11/2}$ level, is largely increased due to energy transfer from Yb^{3+} to Er^{3+}.

The $Yb^{3+} \rightarrow Er^{3+}$ energy transfer efficiency was determined from the decay curves of Yb^{3+}: $^2F_{5/2}$ level for the glass ceramics. For the Er^{3+}/Yb^{3+} co-doped samples, the efficiency of energy transfer can be evaluated by the

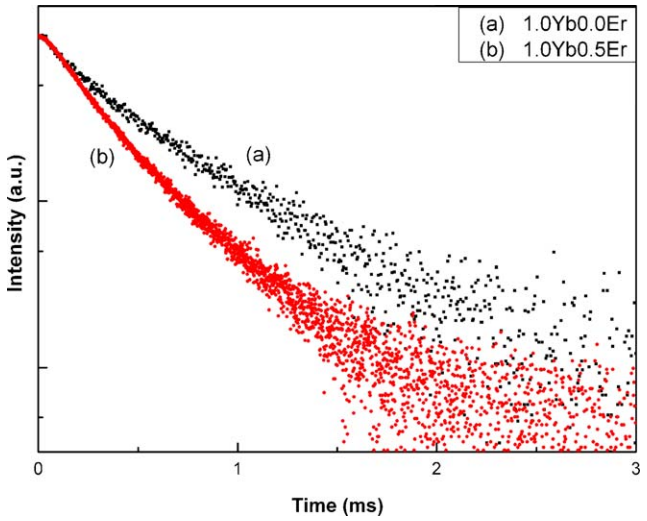

Fig. 8. Fluorescence decay curves of the $^2F_{5/2}$ level of Yb^{3+} for the 1.0Yb^{3+} single-doped and 1.0 Yb^{3+}/0.5Er^{3+} co-doped glass ceramics under 980 nm excitation.

following equation:

$$\eta = \frac{1 - \tau_{Yb/Er}}{\tau_{Yb}} \quad (1)$$

where τ_{Yb} and $\tau_{Yb/Er}$ are the lifetimes of Yb^{3+} ions in Yb^{3+} single-doped and Yb^{3+}/Er^{3+} co-doped samples, respectively. Fig. 8 shows the decay curves of Yb^{3+} ions in the glass ceramics, which exhibit the non-exponential behaviors. The Yb^{3+} ions incorporated in YF_3 nano-crystals are located close to each other, which favors the inter-ionic interactions, and thus leads to efficient non-radiative energy transfer for Yb^{3+}–Yb^{3+} pairs, resulting in the non-exponential decay of the Yb^{3+} emission [16]. Remarkably, the decay of Yb^{3+} in the Yb^{3+}/Er^{3+} co-doped sample is faster than that in the Yb^{3+} single-doped one, which verifies the non-radiative characteristic of the energy transfer from Yb^{3+} to Er^{3+}. The transfer efficiency obtained from Eq. (1) as a function of Yb^{3+} concentration for the glass ceramics with Er^{3+} concentration of 0.1 or

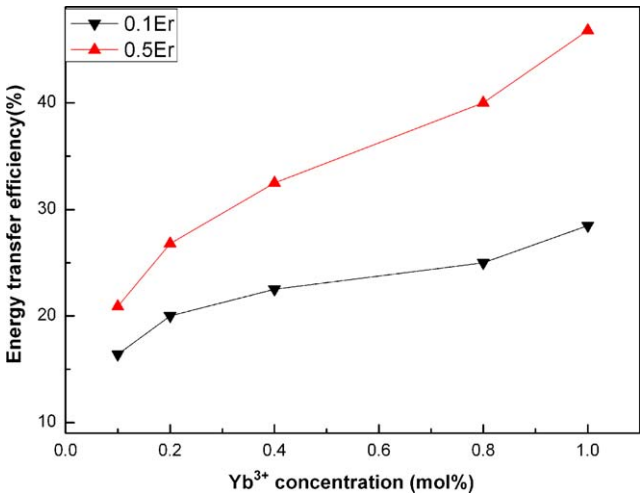

Fig. 9. $Yb^{3+} \rightarrow Er^{3+}$ energy transfer efficiency for the glass ceramics doped with different Yb^{3+} concentration.

0.5 mol%, respectively, is presented in Fig. 9. The energy transfer efficiency increases with increasing of Yb^{3+} concentration, owing to the enhanced inter-ionic interactions between Er^{3+} and Yb^{3+} ions incorporation in YF_3 nano-crystals. The efficiency excesses 45% for the sample of $0.5Er^{3+}/1.0Yb^{3+}$ co-doped glass ceramic.

4. Conclusions

The structure and luminescence of the Er^{3+} single-doped and Er^{3+}/Yb^{3+} co-doped transparent glass ceramics containing YF_3 nano-crystals were investigated. The rare earth ions were confirmed incorporating into the nano-crystals. Compared with Er^{3+} single-doped glass ceramic, the emission intensities of 1.53 μm emission and the infrared to visible up-conversion fluorescence of Er^{3+}/Yb^{3+} co-doped samples under 980 nm excitation were obviously enhanced due to energy transfer from Yb^{3+} to Er^{3+}. The quadratic pump power dependence of the up-conversion green and red emission intensities indicates the two-photon excitation process. The energy transfer efficiency increased with increasing the Yb^{3+} concentration.

Acknowledgements

This work was supported by the National Natural Science Foundation of China (50672098), the Science & Technology Projects of Fujian (2007HZ0002-2, 2008F3114), the projects of CAS (KJCX2-YW-M05) and FJIRSM (SZD07004, 2006K02, 2006KL002) and the Knowledge Innovation Program of CAS and SKLSC (20080039).

References

[1] J.S. Wang, E.M. Vogel, E. Snitzer, Tellurite glass: a new candidate for fiber devices, Opt. Mater. 3 (3) (1994) 187–203.

[2] D. Chen, et al., Broadband near-infrared emission from Tm^{3+}/Er^{3+} co-doped nanostructured glass ceramics, J. Appl. Phys. 101 (11) (2007) 113511–113516.

[3] Y. Kishi, et al., Fabrication and efficient infrared-to-visible upconversion in transparent glass ceramics of Er–Yb co-doped CaF_2 nano-crystals, J. Am. Ceram. Soc. 88 (12) (2005) 3423–3426.

[4] S. Tanabe, et al., Fluorescence properties of Er^{3+} ions in glass ceramics containing LaF_3 nanocrystals, Opt. Mater. 19 (3) (2002) 343–349.

[5] Y.H. Liu, et al., Energy transfer in Yb^{3+}–Er^{3+}-codoped bismuth borate glasses, J. Opt. Soc. Am. B: Opt. Phys. 24 (5) (2007) 1046–1052.

[6] X. Qiao, et al., Luminescence behavior of Er^{3+} ions in glass-ceramics containing CaF_2 nanocrystals, J. Non-Cryst. Solids 351 (5) (2005) 357–363.

[7] D.Q. Chen, et al., Spectroscopic properties of Er^{3+} ions in transparent oxyfluoride glass ceramics containing CaF_2 nano-crystals, J. Phys. Condens. Mater. 17 (41) (2005) 6545–6557.

[8] D.Q. Chen, et al., Partition, luminescence and energy transfer of Er^{3+}/Yb^{3+} ions in oxyfluoride glass ceramic containing CaF_2 nano-crystals, Opt. Mater. 29 (12) (2007) 1693–1699.

[9] M. Abril, et al., Optical properties of Nd^{3+} ions in oxyfluoride glasses and glass ceramics comparing different preparation methods, J. Appl. Phys. 95 (10) (2004) 5271–5279.

[10] Y. Wang, J. Ohwaki, New transparent vitroceramics codoped with Er^{3+} and Yb^{3+} for efficient frequency upconversion, Appl. Phys. Lett. 63 (24) (1993) 3268–3270.

[11] A.S. Gouveia-Neto, et al., Intense red upconversion emission in infrared excited holmium-doped $PbGeO_3$–PbF_2–CdF_2 transparent glass ceramic, J. Lumin. 110 (1–2) (2004) 79–84.

[12] F. Lahoz, et al., Dopant distribution in a Tm^{3+}–Yb^{3+} codoped silica based glass ceramic: an infrared-laser induced upconversion study, J. Chem. Phys. 120 (13) (2004) 6180–6190.

[13] X. Qiao, X. Fan, M. Wang, Luminescence behavior of Er^{3+} in glass ceramics containing BaF_2 nanocrystals, Scr. Mater. 55 (3) (2006) 211–214.

[14] P.A. Tick, Are low-loss glass-ceramic optical waveguides possible? Opt. Lett. 23 (24) (1998) 1904–1905.

[15] H. Guo, Y.M. Qiao, Preparation, characterization, and strong upconversion of monodisperse Y_2O_3: Er^{3+}, Yb^{3+} microspheres, Opt. Mater. 31 (4) (2009) 583–589.

[16] D.Q. Chen, et al., Influence of Yb3+ content on microstructure and fluorescence of oxyfluoride glass ceramics containing LaF3 nano-crystals, Mater. Chem. Phys. 101 (1–2) (2007) 464–469.